High-voltage monitoring with a solenoid retarding spectrometer at the KATRIN experiment

2014 JINST 9 P06022

(http://iopscience.iop.org/1748-0221/9/06/P06022)

PUBLISHED BY IOP PUBLISHING FOR SISSA MEDIALAB

RECEIVED: *December 9, 2013*
REVISED: *March 28, 2014*
ACCEPTED: *May 1, 2014*
PUBLISHED: *June 26, 2014*

High-voltage monitoring with a solenoid retarding spectrometer at the KATRIN experiment

M. Erhard,[a,1] **S. Bauer,**[b,2] **A. Beglarian,**[a] **T. Bergmann,**[a] **J. Bonn,**[c,3] **G. Drexlin,**[a] **J. Goullon,**[a] **S. Groh,**[a] **F. Glück,**[a,d] **M. Kleesiek,**[a] **N. Haußmann,**[a] **T. Höhn,**[a] **K. Johnston,**[e] **M. Kraus,**[a] **J. Reich,**[a] **O. Rest,**[b] **K. Schlösser,**[a] **M. Schupp,**[a] **M. Slezák,**[f,g] **T. Thümmler,**[a] **D. Vénos,**[g] **C. Weinheimer,**[b] **S. Wüstling**[a] **and M. Zbořil**[b,2]

[a] *KCETA, Karlsruhe Institute of Technology, D-76131 Karlsruhe, Germany*
[b] *Institute for Nuclear Physics, University of Münster, D-48149 Münster, Germany*
[c] *Institute for Physics, Johannes Gutenberg University of Mainz, D-55099 Mainz, Germany*
[d] *Wigner Research Institute for Physics, H-1525 Budapest, POB 49, Hungary*
[e] *Physics Department, CERN, CH-1211 Geneva, Switzerland*
[f] *Faculty of Mathematics and Physics, Charles University of Prague, CZ-12116 Prague, Czech Republic*
[g] *Nuclear Physics Institute of the ASCR, CZ-25068 Řež near Prague, Czech Republic*

E-mail: moritz.erhard@kit.edu

ABSTRACT: The KATRIN experiment will measure the absolute mass scale of neutrinos with a sensitivity of $m_\nu = 200\,\mathrm{meV/c^2}$ by means of an electrostatic spectrometer set close to the tritium β-decay endpoint at 18.6 keV. Fluctuations of the energy scale must be under control within ± 60 mV (± 3 ppm). Since a precise voltage measurement in the range of tens of kV is on the edge of current

[1] Corrisponding author.
[2] Present address: Physikalisch Technische Bundesanstalt, D-48149 Münster, Germany
[3] Deceased.

doi:10.1088/1748-0221/9/06/P06022

2014 JINST 9 P06022

technology, a nuclear standard will be deployed additionally. Parallel to the main spectrometer the same retarding potential will be applied to the monitor spectrometer to measure 17.8-keV K-conversion electrons of ^{83m}Kr. This article describes the setup of the monitor spectrometer and presents its first measurement results.

KEYWORDS: Real-time monitoring; Spectrometers; Control systems

Contents

1 Introduction

The purpose of the KArlsruhe TRItium Neutrino (KATRIN) experiment is to determine the effective mass[1] of the electron anti-neutrino by measuring the electron spectrum of tritium beta-decay close to its endpoint (ref. [1]). The sensitivity will be improved from currently 2 $\mathrm{eV/c^2}$ (ref. [2]) to 200 $\mathrm{meV/c^2}$ (90 % CL). The energy of electrons emitted by gaseous tritium is analyzed with the KATRIN main spectrometer based on Magnetic Adiabatic Collimation and an Electrostatic filter (MAC-E filter) (ref. [3]).

MAC-E filters have the advantage that they can operate with a large source area and accept a large solid angle so that the low intensities at the end point (the decay rate in the last 1 eV is only a fraction of $2 \cdot 10^{-13}$ of the total decay rate) can be compensated. Also, a very high energy resolving power of $E/\Delta E = 20000$ can be realized for KATRIN at the cost of being an integrating spectrometer. Close to the endpoint of a beta spectrum the integrating feature is not a drawback at all.

However, it must be ensured that the retarding potential corresponding to the 18.6 keV tritium endpoint-energy (ref. [4]) is stable and reproducible for at least one measurement period of two months or more. To achieve the designed neutrino mass sensitivity of 200 $\mathrm{meV/c^2}$, a stable retarding potential of ± 60 mV at 20 keV (± 3 ppm) is required within a KATRIN run (ref. [1]). The effect of voltage-scale imperfections on results of a neutrino-mass measurement from beta-decay was studied in ref. [5].

[1] The observable is actually an incoherent sum of the neutrino mass eigenstates m_i, where U_{ei} are the corresponding elements of the Pontecorvo-Maki-Nakagawa-Sakata leptonic mixing matrix $m_{\bar{\nu}_e} = \sqrt{\sum_{i=1}^{3} |U_{ei}|^2 \cdot m_i^2}$.

2014 JINST 9 P06022

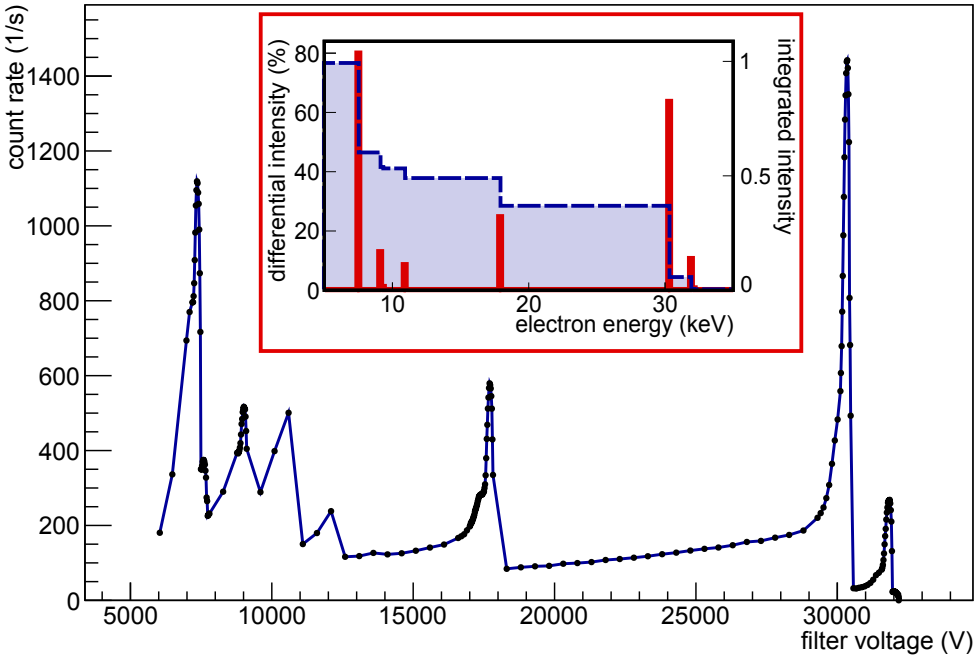

Figure 1. The ^{83m}Kr conversion-electron spectrum measured with the monitor spectrometer. The lines at about 10.4 keV and 12.0 keV are identified with Auger-electrons. For further information see ref. [14]. The insert illustrates the electron energies and intensities taken from ref. [15]. The solid red lines represent the differential energy spectrum, and the integration of those values is shown as a dashed blue line.

The requirement for an absolute accuracy to compare a measured tritium endpoint with a determined value by a Penning-trap mass spectrometer (ref. [6, 7]) can be used to reduce systematic uncertainties. Relative accuracy is more demanding, therefore a high-voltage drift must be avoided and fluctuations suppressed.

To do so, state of the art high-voltage measurement techniques will be deployed (ref. [8, 9]). A high-voltage supply system is used which is stable at below a level of 10 ppm/8 h. This high voltage is monitored with a custom-made high voltage divider (ref. [10, 11]), since there is no of-the-shelf solution to measure a voltage in the multi kV regime with ppm precision. The stability of those high-precision dividers is world leading and allows an absolute high-voltage measurement on a ppm level. In order to smooth out high-frequency disturbances that can be imposed, capacitors and a triode shunt for an active voltage regulation are utilized.

An additional and completely different method of monitoring the retarding potential is to compare it with a nuclear standard, an emitter of mono-energetic electrons. These are measured with the monitor spectrometer, a further MAC-E filter. The retarding electrode-systems of the monitor spectrometer and the main spectrometer are galvanically connected during calibration runs and neutrino-mass measurement. Therefore both spectrometers are operated with the same retarding potential and measurement method to reduce systematic uncertainties and to determine a reference value of the retarding potential. A change of electron energy measured at the monitor spectrometer will indicate a problem in the high voltage measurement. In such a way, jumps and larger drifts of the main spectrometer voltage can be identified and tritium data assessed.

2014 JINST 9 P06022

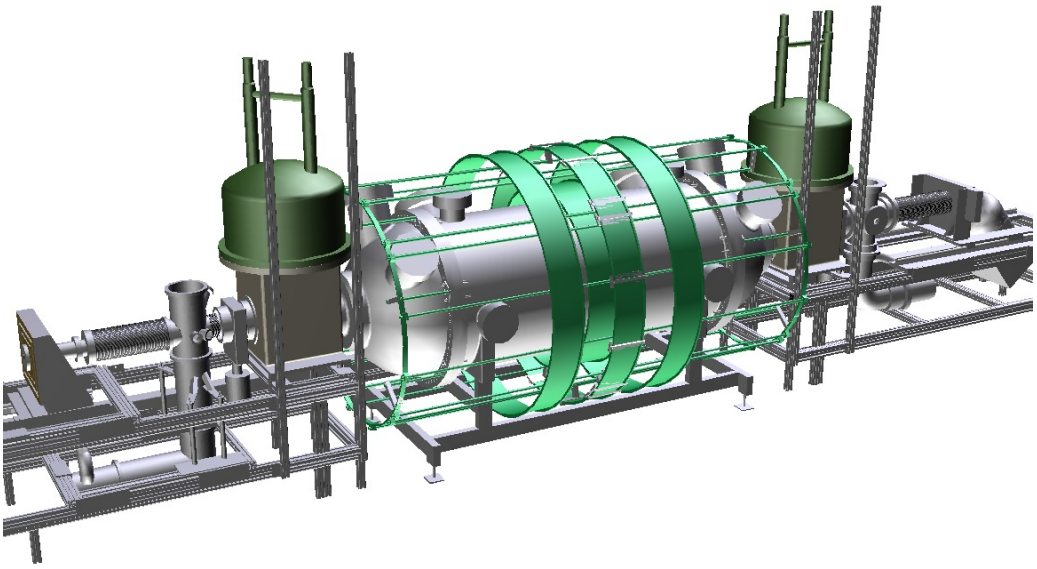

Figure 2. Monitor spectrometer setup. The source is placed in a vacuum chamber on the left side of the superconducting solenoid (grey housing with green dome). The detector is placed on the right side in a similar way. In the center, a set of four axial copper air coils on aluminum formers to adjust the magnetic field in the analyzing plane is mounted. The earth magnetic field compensation system is realized with insulated, horizontal copper pipes (both in light green).

In the search for a suitable mono-energetic electron source, conversion electrons emitted by a ^{83m}Kr decay with an energy of 17.8 keV close to the tritium endpoint showed most promising results. To adjust the nuclear standard to the retarding potential the source is biased by an auxiliary power supply. For continuous monitoring a source is preferred where ^{83m}Kr ($t_{1/2}$ = 1.86 h) is continuously produced by electron-capture decay of ^{83}Rb ($t_{1/2}$ = 86.2 d), implanted into a solid substrate (ref. [12]). The retention of ^{83m}Kr is about 90 %, so only 10 % does not decay within the source material (ref. [13]).

In order to measure the electron energy-spectrum of ^{83m}Kr (ref. [14, 15]), the apparatus of the former Mainz neutrino experiment (ref. [16]) was simplified, refurbished and reassembled in Karlsruhe. Due to the integrating feature of the spectrometer, a high background would be expected for electrons beneath electron lines of higher energies (figure 1 insert). This is widely overcome by using a PIN-diode as electron detector with sufficient resolution to separate high and low energies. Furthermore, electrons with high surplus energies with respect to the retarding potential are collimated poorly onto the detector, due to their non-adiabatic movement (ref. [17, 18]). The whole energy spectrum of ^{83m}Kr looks contrary to the expected step-like shape of an integrating spectrometer (figure 1). A detailed discussion of the ^{83m}Kr electron energy spectrum can be found in ref. [12, 19].

2 Spectrometer setup and measurement principle

A drawing of the refurbished spectrometer is shown in figure 2. Two superconducting solenoids on both ends and four air coils in the center of the spectrometer generate an axially symmetric

2014 JINST 9 P06022

magnetic field. The distance between the centers of the solenoids is 4.02 m and the inner diameter of the vacuum tank is 1 m. In the tank are solid filter electrodes and a wire electrode system. The area of the usable analyzing plane has a radius of about 0.35 m.

The source and detector magnets as they were present in the Mainz setup are not used anymore. The source magnets were used for the tritium source[2] and are no longer needed as for monitoring a simple metal foil as a solid substrate is used, in which the nuclear standard is embedded. A detector magnet allowed to adjust the size of the source image on the detector and ensured that the field lines impinge perpendicular. In the new setup small solid sources and a smaller detector are used (section 2.4), so that the problem of oblique field lines on the detector is of little concern. Also, additional lead shielding for background reduction, placed inside the detector magnet, is not required any longer since the installed sources provide high count rates of mono-energetic electrons compared to the background.

The stainless-steel electrode system of the monitor spectrometer is installed in the same way as it was in the original Mainz setup (ref. [18]). While the vessel is grounded, a retarding potential can be applied to a system of cylindrical and conical full-metal electrodes as well as two wire electrodes. In the original setup, a voltage difference of a few hundred volts between the wire electrodes was used to reduce induced background from cosmic rays (ref. [20]). High count rates at the monitor spectrometer make this method dispensable, but to facilitate further background studies, the wire electrodes were kept.

In this paper only a brief introduction to the MAC-E-filter measurement technique is given, for further details the reader is referred to ref. [1] and ref. [3]. In order to describe the monitor spectrometer, a right-handed coordinate system is used that has its origin in the center of the spectrometer tank. The z-axis points axially to the detector, the y-axis describes the vertical and the x-axis the horizontal alignment directions.

The main magnetic field is created by two superconducting solenoids with a maximum field of 6.014 T (50 A) and four air coils in the center, the so-called Low Field Correction System (LFCS). The two outer air coils are set to -18 A, the outer center coil to -8.8 A and the inner center coil to 5 A. The plane in the center perpendicular to the spectrometer axis is called the analyzing plane, in which the resulting field is minimal at a value of 309 μT. This setting (ref. [18]) was used for almost all recent ^{83m}Kr measurements in Mainz (ref. [22, 23]).

The magnetic field of a MAC-E filter guides electrons emerging from a source through the spectrometer to a detector. Within the spectrometer the magnetic field strength decreases, leading to an adiabatic transformation of the transverse motion into a longitudinal one, so that an electrostatic potential can act as a high-pass energy filter. A sketch of the electromagnetic system and calculated magnetic field lines are shown in figure 3. Calculations were performed with KASSIOPEIA the KATRIN particle tracking and electromagnetic field-calculation package (ref. [21]).

Electrons starting from the source perform a cyclotron motion superimposed to their longitudinal movement towards the magnet on the source side. The motion can be assumed to be adiabatic when the magnetic field changes only slightly over one cyclotron revolution, the associated mag-

[2]The tritium-source magnets were tilted to each other to increase the differential pumping performance that reduces a residual tritium flow into the spectrometer.

2014 JINST 9 P06022

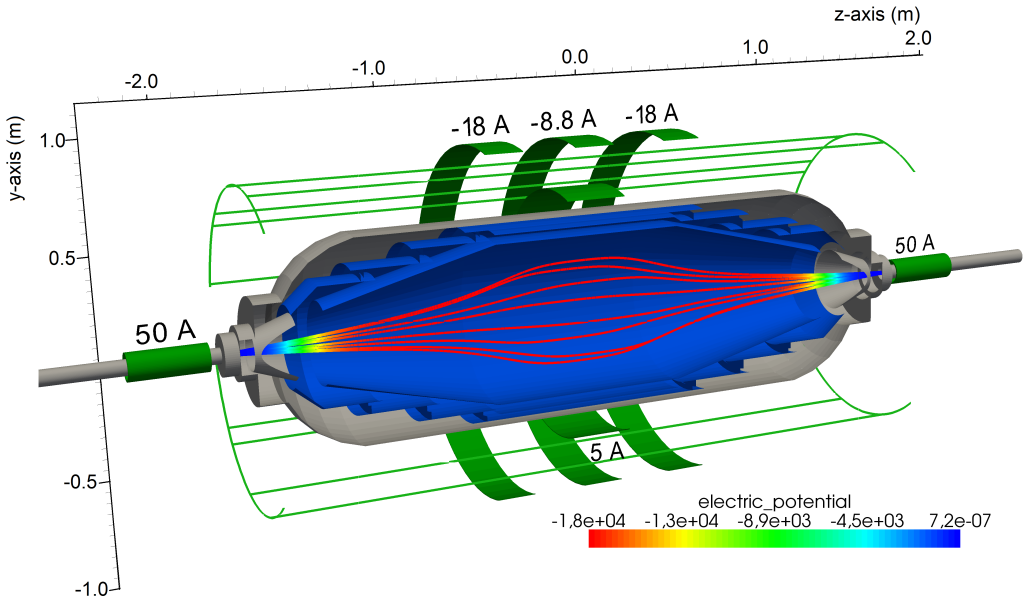

Figure 3. Electromagnetic configuration of the monitor spectrometer. The spectrometer vessel and the conical ground electrodes are kept on ground potential (grey), the stepped cylindrical massive electrode and the wire electrode are on common high voltage (blue), which covers almost the entire inner surface. Also the magnet coils (green) and their corresponding currents are shown (currents of earth magnetic field compensation not included). Along a few selected magnetic field-lines, the color-coded magnitude of the electric potential is visualized. Magnetic field lines start at the source position most commonly used for measurements. Covering a source radius of 3 mm, the corresponding radius in the analyzing plane, is 25 cm.

netic moment

$$\mu = E_\perp / B \tag{2.1}$$

is preserved (equation given in non-relativistic limit). Consequently the transversal energy $E_\perp$ of the electrons decreases as they move from a high magnetic field to the analyzing plane. A static magnetic field implies energy conservation so that $E_\perp$ is transformed into longitudinal energy $E_\parallel$.

With an additional electrostatic potential, electrons can pass the analyzing plane if their longitudinal energy is larger as an effective potential U_f

$$E_\parallel > -\mathrm{e}U_\mathrm{f}, \tag{2.2}$$

where e represents the elementary charge. An applied potential U_0 is altered by the spectrometer work-function ϕ_spec and a radial and potential depending punch-through U_rad

$$-\mathrm{e}U_\mathrm{f} = -\mathrm{e}U_0 + \phi_\mathrm{spec} - \mathrm{e}U_\mathrm{rad}(r, U_0). \tag{2.3}$$

The precise value of the work function (≈ 4.5 eV for stainless steel) highly depends on the surface condition of the electrode system. As a result of the finite length of the spectrometer, the potential in the analyzing plane is affected by the grounded electrodes on both ends of the spectrometer. Therefore electrons experience a slightly more positive potential close to the spectrometer axis. For a larger potential the effect is more pronounced. In the spectrum analysis (section 3) this effect

2014 JINST 9 P06022

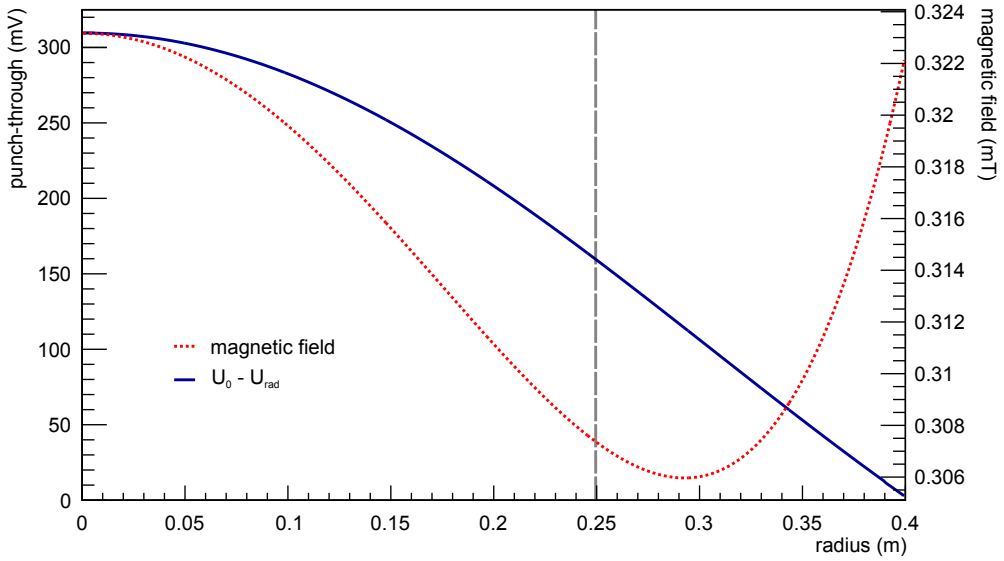

Figure 4. Radial dependency of the punch-through (left axis) and the magnetic field (right axis) in the analyzing plane. The vertical grey line is the maximal radius for electrons starting on a 3-mm radius from the most common source position. The calculations were performed with a potential of $U_0 = -17825$ V. The used magnetic field values are based on the currents presented in figure 3.

is taken into account. Figure 4 shows the calculated radial potential dependence in the analyzing plane relative to an applied potential of $U_0 = -17825$ V. On the spectrometer axis $r = 0$ m the potential U_0 is shifted by $U_{\text{rad}} = 310 \pm 16$ mV with an assumed uncertainty of 5 %.

The used magnetic field setting (ref. [18]) of the monitor spectrometer setup was developed to fulfill certain criteria. Since the magnetic field in the analyzing plane is non zero, the same holds for the transversal energy. This fact leads to finite energy resolution and eq. (2.1) then reads

$$\mu = E_{\text{tot}}/B_{\text{max}} = \Delta E/B_{\text{ana}}. \tag{2.4}$$

Here ΔE has been identified with $E_\perp$ in the analyzing plane and E_{tot} with $E_\perp$ in the maximum field. Hence, the relative energy resolving power is

$$\frac{E_{\text{tot}}}{\Delta E} = \frac{B_{\text{max}}}{B_{\text{ana}}} = \frac{6.014\ \text{T}}{309\ \mu\text{T}} = 19463, \tag{2.5}$$

this results in an energy resolution of $\Delta E = 0.93$ eV at 18.6 keV.

Beside providing a high energy resolution, another requirement is a magnetic field inhomogeneity that does not exceed 10 % in the covered flux tube and a non-adiabatic electron transport should be avoided (ref. [18]). In figure 4 the radial dependence of the magnetic field is plotted as well. Within the covered flux tube, the magnetic field inhomogeneity adds up to 4.7 %.

Finally, the adiabatic energy transformation leads to a maximum acceptance angle. Electrons are emitted from the source with an isotropically distributed angle θ with respect to the magnetic field. According to eq. (2.1) the transversal energy increases while the electrons move towards a

high magnetic field in the center of the source side magnet. Only if some forward energy is left they are transmitted to the spectrometer. The maximum acceptance angle is given by

$$\sin\theta_{\max} = \sqrt{\frac{B_S}{B_{\max}}}, \tag{2.6}$$

where B_S is the field at the site of the source and $B_{\max}$ in the center of the superconducting magnet. Electrons starting with the maximum acceptance angle just pass the magnet on the source side and get their total energy transformed into cyclotron motion at the maximum field.

2.1 High voltage (HV)

High-voltage up to 35 kV can be obtained either from a local supply or from the main spectrometer HV system (figure 5). For the measurement period presented here, the monitor spectrometer is operated in a standalone mode (red components in figure 5). This means that the potential of the monitor spectrometer is generated by a separate voltage supply, scaled down by the ppm-precision high-voltage divider K35 (ref. [10]) and measured by a high-precision digital voltmeter[3].

In a normal KATRIN operation the monitor spectrometer is embedded in the overall KATRIN high-voltage scheme (red and blue components in figure 5). During tritium data taking it is planned to apply the same fixed potential of one common power supply to the inner wire electrode of the main spectrometer and to the electrodes of the monitor spectrometer. The spectrometers are connected individually to one of the KATRIN ppm-precision high-voltage dividers (ref. [10, 11]). A high-voltage distribution is chosen to enable an electron-energy measurement by either variate the source potential or the retarding potential of the spectrometer. Depending on the requested method a different read-out configuration has to be used.

If the scan of the electron spectrum is done by changing the potential of the tritium source while the retarding potential at main and monitor spectrometer is constant, a varying bias has to be applied to the implanted krypton source of the monitor spectrometer (section 2.5). Since the absolute value of this bias potential is less than 1 kV, a commercial reference divider[4] can be used to scale this voltage down to be measured with a high-precision digital voltmeter.

For calibration runs of the KATRIN main setup krypton will be utilized as gas in the source or as condensed layer on a substrate in the transport section (ref. [1]) and compared with krypton measurements at the monitor spectrometer. The high-voltage connection between main spectrometer and monitor spectrometer remains the same as for tritium data taking. Also in this case the source voltages of both spectrometers are varied. A detailed description of the KATRIN high-voltage system, its capabilities and requirements is in preparation.

2.2 Magnetic field system

To ensure axial symmetry the background field needs to be compensated, in particular the earth magnetic field of $\approx 50\ \mu$T. This is accomplished by two coil sets called Earth Magnetic field Compensation System (EMCS). One set produces a vertical magnetic field, the other a horizontal one, both being perpendicular to the spectrometer axis. The winding geometry is chosen to follow

[3] A Fluke 8508 voltmeter is used not only for measurements presented in this paper, but during neutrino-mass measurements as well.

[4] The Model is a Fluke 752A.

2014 JINST 9 P06022

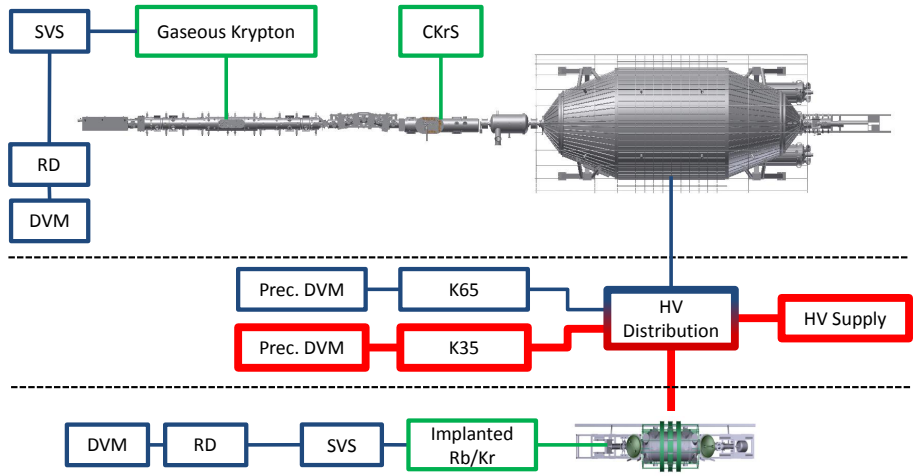

Figure 5. Schematic overview of the high-voltage monitoring concept. Both spectrometer electrodes are supplied by the same high voltage by a precision high-voltage power supply (HV supply). This retarding potential is redundantly monitored by the KATRIN high-precision voltage dividers (K35 and K65) (ref. [10, 11]) and precise voltmeters (Prec. DVM) as well as by the monitor spectrometer. In order to measure the conversion electron line K-32, the implanted krypton source can be biased via a dedicated power supply (SVS). This bias voltage will be monitored by a Fluke 752A reference divider (RD) and a digital voltmeter (DVM). The applied precision digital voltmeters are Fluke 8508 and Agilent 3458A. Additionally to the monitor spectrometer the energy calibration can be carried out via krypton admixture in the windowless gaseous tritium source (WGTS) or by the condensed krypton source (CKrS) inside the cryogenic pumping section. A voltage can be applied on the WGTS comparable to the monitor spectrometer, while the readout is similar to the monitor spectrometer. For the current measurements at the monitor spectrometer only the HV equipment in bold red lines was used.

a $\cos(\Theta)$ distributed current pattern (ref. [24, 25]), with four windings for the horizontal and the vertical field directions each.

For tests of the magnetic field with a fluxgate sensor the coil system was assembled standalone, oriented in East-West direction to inhibit an axial component of the earth magnetic field. The spatial distribution of the residual field with optimized EMCS currents is shown in figure 6.

In order to find proper EMCS settings and to check the LFCS, the field was measured again in the final position when all air coils were installed on the tank and before the superconducting solenoid at the detector was mounted. The measurements are shown in figure 7, for which a fluxgate sensor on a vertical guide rail was inserted and aligned along the spectrometer axis. Only in the center a full compensation is obtained whereas along the z-axis some residual field remains. This is caused by the bolts used to connect the cylindrical part and domes on both spectrometer tank-ends. These bolts are made of normal magnetic steel to withstand the required torque to get the spectrometer vacuum tight. However, this deterioration of 10 μT occurs in a region where the 5 mT field of the superconductors are dominating.

The field produced by the entire air-coil system was also measured and the results are shown in figure 8, where some unexpected perpendicular components appear (B_x and B_y). Since the actual sensor position is only known within $< 0.5^\circ$ and < 2 cm, field calculations were performed to check if the deviation could be attributed to a small misalignment of the guide rail for the fluxgate

2014 JINST 9 P06022

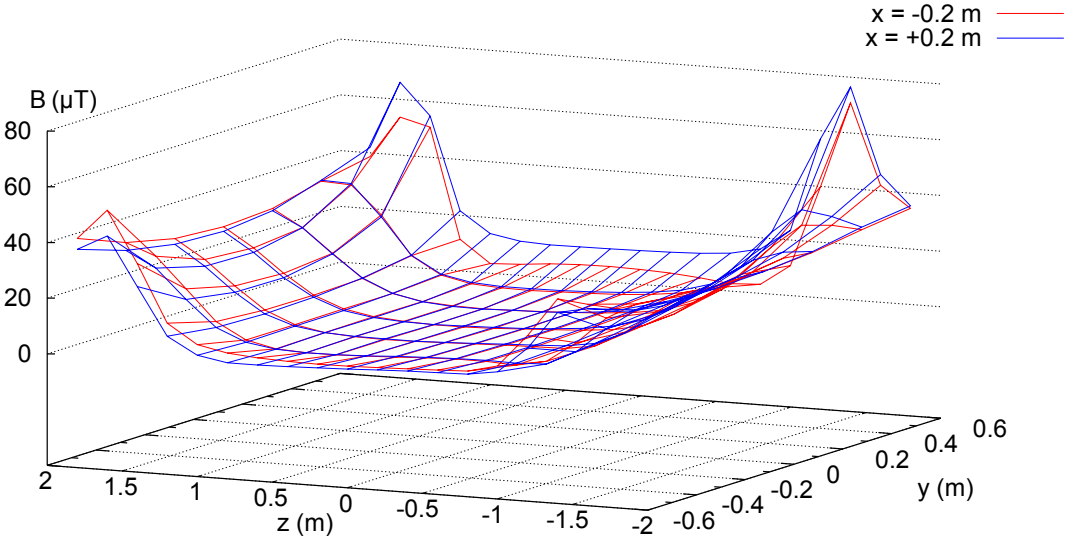

Figure 6. Spatial residual field distribution of the earth magnetic field compensation system. The currents were tuned to compensate the background field in the center. The field was measured in the z-y plane once $+20$ cm (blue) from center and once -20 cm (red). It is compensated within ± 1.5 m upstream and downstream the analyzing plane and within the radius of the spectrometer tank of 0.5 m. Outside that region, the fields of the superconductors are by far dominating.

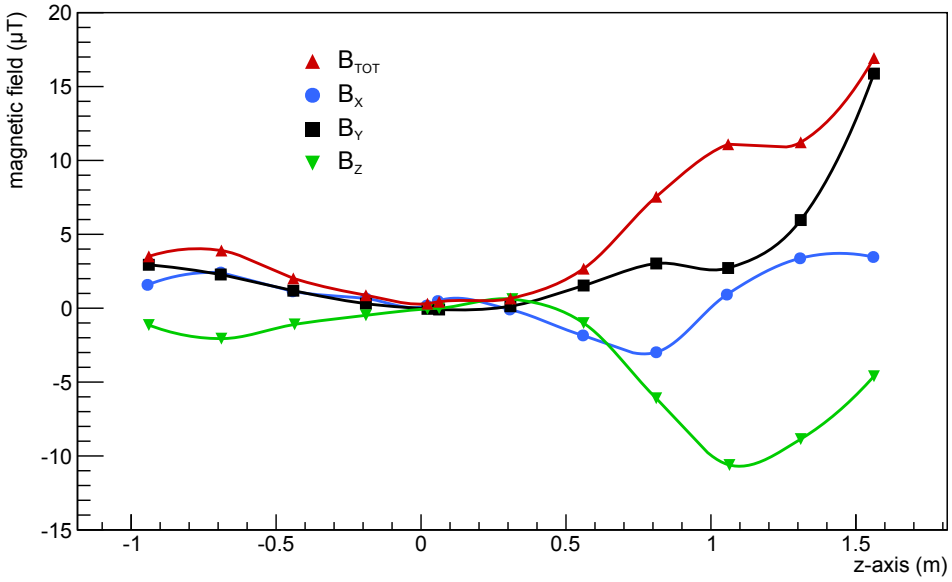

Figure 7. Magnetic background field compensated by the earth magnetic field compensation system and the outer low field correction system air coils. These coils compensated the axial-component at $I = 445$ mA. The magnetic field increases for larger z values, but this is negligible since the field is dominated by the solenoids in these regions (at $z = 1$ m the field of the solenoids is about 5 mT).

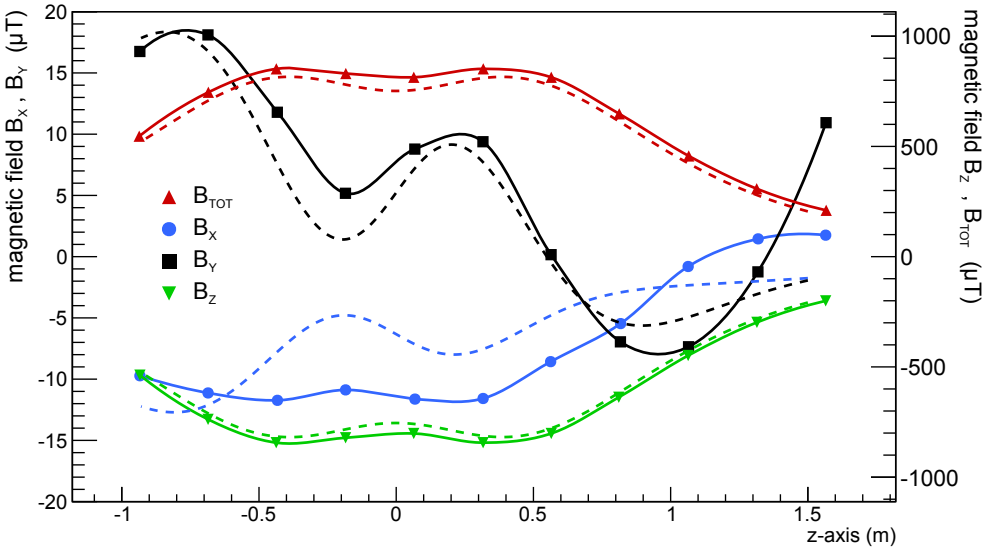

Figure 8. Magnetic field with live earth magnetic field compensation system (EMCS) and low field correction system (LFCS). The horizontal EMCS is operated at $I = 1.51$ A, the vertical at $I = 19.5$ A. The LFCS is operated as presented in figure 3. B_x and B_y are plotted on the left axis, B_z and B_{total} on the right one. The dotted lines are the corresponding field calculations.

sensor. For the field calculation in figure 8 a sensor offset of $x = -0.01$ cm and $y = 0.02$ cm and a tilting to the x-axis of 0.3° and to the y-axis of -0.4° was used. Under these preconditions the calculated and measured absolute field values agree within 97 %.

Finally, the far field of the superconducting coils was measured along a representative line parallel to the spectrometer axis at a distance of about 0.684 m from the axis. The results are shown in figure 9 together with calculations performed with KASSIOPEIA. Magnetic field calculations confirm the measurements at the side of the source, but a significant deviation is observed for the magnet at the detector side. Analysis of the measured stray field points to a small misalignment of the superconducting coil with respect to spectrometer axis. Based on this measurement alone, it is not possible to determine the true characteristics of the misalignment. For this purpose a near-field measurement of the magnet is necessary which is on the agenda for an upcoming spectrometer shutdown. Nevertheless it was attempted to compensate the imperfections by the EMCS empirically. The results are presented in section 3, figure 13.

The relation given by eq. (2.5) holds only for electrons on the z-axis. Due to small inhomogeneities in the analyzing plane of the magnetic and electric fields, caused by potential punch-through and a small radial gradient of the magnetic field, the total resulting resolution is slightly worse. A detailed calculation with KASSIOPEIA which takes into account all disturbances mentioned in this section yields a resolution of about $\Delta E = 1.1$ eV.

2.3 Vacuum system

To avoid energy losses of the conversion electrons and the production of secondary electrons, due to inelastic scattering with residual gas, an ultra-high vacuum (UHV) is required (ref. [26]). Com-

2014 JINST 9 P06022

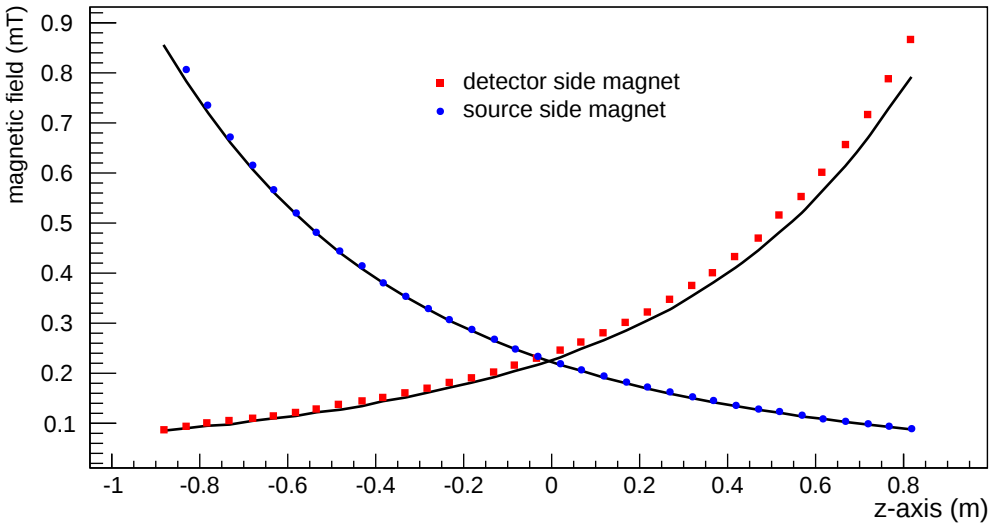

Figure 9. Far field measurement of the superconductors which were operated at a nominal field of 3.007 T, both measured separately. Only the absolute value of the field is shown, because this is insensitive to small angular misalignments. The background field is subtracted. The comparison to KASSIOPEIA calculations are plotted in black lines.

pared to the main spectrometer-vacuum, conditions are less critical, since high intensities and an inevitable background from conversion electrons with higher energies exist.

Ultra-high vacuum in the monitor spectrometer is created and maintained by cascaded turbo-molecular pumps, as illustrated in figure 10. The spectrometer tank, the detector and the source chamber are each equipped with a turbo pump, connected to a common fourth one in order to maintain a high vacuum in the lower 10^{-7}-mbar regime. The intermediate turbo pump is backed by a 5 m^3/h scroll pump. The fore vacuum volume is enlarged by a buffer vessel of about 110 l, allowing intermittent operation of the scroll pump controlled by the PCS7 system (section 2.6). A scroll-pump operation time of less then 30 min/d has the advantage of lower maintenance costs[5], a reduced average noise level and it is ensured that most decays of gaseous ^{83m}Kr take place within the buffer volume.

For simplicity there are no separate source or detector magnets, as described in section 2. To achieve a sufficient magnetic field strength, the sources and detector have to be moved into their respective gate valves (figure 10). These valves must not be closed although that would be preferred in case of a failure. In order to preserve UHV in the tank even without electricity, pneumatic valves in front of all pumps are installed closing automatically by compressed air when electricity fails.

The pressure in the detector chamber is about two orders of magnitude higher than in the spectrometer tank. It contains soldered electronics, the first field-effect transistor amplifier stage, which can only be exposed to temperatures < 70 °C, and hence only a moderate bake-out is possible. Even more, the turbo pump at the detector chamber has to be switched off during measurements, because it generates micro-phonics by vibrations that spoils the signal. The situation is somewhat eased by cooling the detector and the first amplifier stage in the vacuum with liquid nitrogen. The

[5]The maintenance interval is 8000 h.

2014 JINST 9 P06022

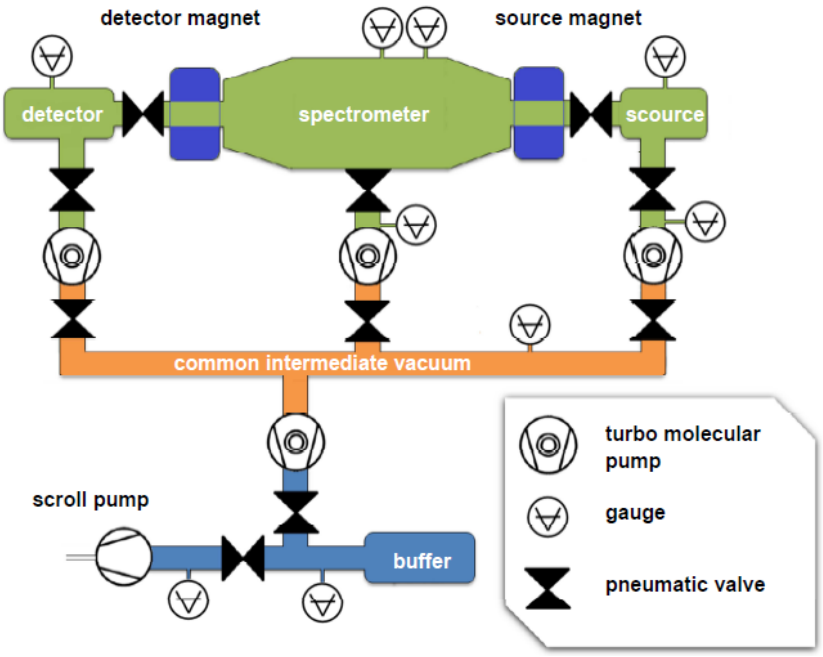

Figure 10. Scheme of the vacuum system. The UHV section is indicated by green color, high vacuum by orange and the fore vacuum by blue. Only the pneumatic valves are shown. There are additional hand valves on each chamber and on the back of each turbo pump to connect an auxiliary pump or a leak detector. The spectrometer tank is instrumented with a wide range gauge and an extractor gauge which is sensitive down to 10^{-12} mbar.

relatively large cold surface of the cold finger and electronics works as a cryogenic pump, and also the detector chamber is pumped through the gate valve to the tank. Due to a collimator, 250 mm long and 25 mm in diameter, load on the tank vacuum is only in the order of $2 \cdot 10^{-7}$ mbar l/s. Typically the pressure at the detector is still $< 5 \cdot 10^{-8}$ mbar and at the tank $1.4 \cdot 10^{-10}$ mbar.

The line position of the conversion electrons from the ^{83}Rb/^{83m}Kr source (ref. [12]) is very sensitive to the filter-electrode condition, e.g. after a vacuum failure a thorough bake out is necessary to remove adsorbed gases and humidity from all inner surfaces. Otherwise the altered electrode work function shifts the measured line position by a few hundred meV. Special emphasis has been put on the heating system to enable a heat cycle up to 200 °C in a conveniently short time. Most heating elements from the Mainz setup could be reused, while a new thermal spectrometer insulation was installed. Two big bellows allow a movement of the source and the detector without breaking vacuum, for those bellows demountable insulated heating elements were fabricated. About 80 Pt100 thermometers and 15 heating circuits are mounted on the spectrometer and are connected to the PCS7 slow control system, enabling fully automated heating cycles. Usually the temperature is changed with a rate of 0.2 K/min (heating and cooling) which is slow enough to avoid too high temperature gradients. After several months of monitoring, the effectiveness of the heating process has been tested (section 3).

2014 JINST 9 P06022

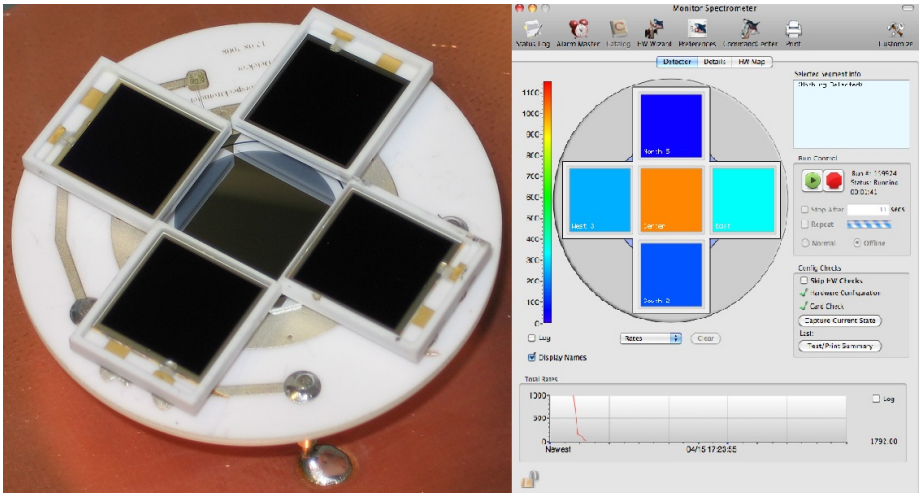

Figure 11. Photo of the detector (left) and as it appears in the DAQ (section 2.6) (right). The colors indicate the respective count rates. To minimize the dead zone between the central pixel and the outer ones, the ceramics backing of rectangular diodes had been cut on the side adjacent to the central pixel. The outer diodes are not in the same plane with the central one, but a little elevated, so that they can overlap the center.

2.4 Detector

As detector, a circular silicon PIN-diode with a sensitive area of 1.5 cm^2 and a depletion depth of 0.5 mm was chosen (Canberra PD-150-12-500AM). As auxiliary detectors, four small quadratic windowless PIN-photo diodes (Hamamatsu S3590-09) are mounted around the central one to facilitate centering in the electron beam (figure 11). The existing electronics from Mainz were overhauled and the circuit-boards of the warm preamplifier stage were rebuilt according to the previous design (ref. [27]).

The detector and the first pre-amplifier stage are mounted inside the vacuum chamber on a copper-beryllium rod, used for its enhanced mechanical properties compared to pure copper. To use the rod as a cold finger the lower specific heat conductivity is compensated by an appropriate thicker diameter. The rod is attached to an actual cold finger of copper, supported by a stainless steel tube and fed through a base flange outside the vacuum chamber where it is immersed into liquid nitrogen. The resulting detector temperature[6] of ≈ -45 °C leads to an acceptable electronic noise level.

The base flange is mounted in a cross table and connected to the vacuum chamber by a diaphragm bellows. The cross table allows vertical and horizontal movements of ± 10 mm and is mounted on a chariot to allow axial movement. This setup gives the flexibility to align the detector on axis and to select a magnetic field by axial movement in vacuum conditions. To perform a detector alignment onto the magnetic axis a reversed magnetic field value in the analyzing plane is chosen, so that field lines connect the auxiliary detectors with the filter electrode on HV. This setting gives a convenient count rate of secondary electrons from the filter electrode, appearing at the detectors with an energy corresponding to a multiple of the filter voltage. Alignment is achieved when all count rates of the auxiliary detectors are balanced.

[6]The temperature is measured with a Pt100 mounted on the first pre-amplifier stage, right behind the detector pixels.

2014 JINST 9 P06022

2.5 Source section

The actual source is an ^{83}Rb ion implanted substrate, based on the results of ref. [12]. As a source holder, a ceramic disk with slots for up to 4 sources is used. The slots are 4-mm banana sockets where a custom-made source case can be plugged in. Each slot, individually connected with a PTFE coated cable to a feedthrough, can be biased up to -770 V to bridge the gap between the K-32 energy of ≈ 17830 eV and the tritium endpoint of ≈ 18600 eV.

The source holder is mounted on an insulated tip of a long tube welded into the base flange. To allow movement in axial direction the base flange is mounted in a cross table, similar to the detector setup. A cross table latitude of ± 20 mm in vertical and horizontal direction was chosen corresponding to source positions arranged in a circle of 20 mm diameter.

In order to align a source with respect to the source solenoid axis, a rotatable scanner is installed in between the source solenoid and the spectrometer. The scanner is a fork with two blades and is actuated by a piezo motor (ANR101/RES/UHV by Attocube Systems AG) compatible to UHV conditions and high magnetic fields. The blades of the scanner can be moved into the electron beam and stop the electrons in a particular section of the flux tube. At two known angles it will either block the electron beam horizontally at $y = 0$ mm or vertically at $x = 0$ mm. This allows horizontal and vertical scanning by only one axis of rotation. When a suitable rotation of the scanner is performed the count rate decreases when a blade enters the flux tube. After the scan of the first blade the count rate restores to its original value until the second one enters. The principle of operation and measurement results demonstrating its capabilities are shown in figure 12. In this measurement only the horizontal source position is aligned whereas the vertical direction is off-axis. Also a picture is included, taken during the monitor spectrometer commissioning. It shows the magnet of the source section from the spectrometer tank side. The scanner and the motor are mounted at the flange connecting the magnet and the spectrometer tank, close to the electron beam line.

Since the scanner can be moved close to or even into the beam it can collect stored electrons, therefore it acts similar to the sweeping wire described in ref. [28]. Charged particles are confined in a MAC-E-filter setup radially within a given magnetic flux tube when conservation according to eq. (2.1) is fulfilled. In longitudinal direction, they are stored in a magnetic bottle where particles are reflected by a magnetic field according to eq. (2.6), in a penning trap reflected by electrostatic potential extremes[7] and by a combination of these two mechanisms. Investigations on several methods to remove stored particles were performed with the pre-sprectrometer test setup (ref. [28, 29]).

2.6 Slow control and Data Acquisition (DAQ)

The monitor spectrometer has to be integrated into the KATRIN environment and therefore has to follow the given hardware and software structure by the overall KATRIN strategy.

A basic function of the slow control is to ensure safe and reliable hardware operation especially for tritium involving components, therefore the well established PCS7 control system by Siemens Inc. is employed throughout the experiment. Considered as basic functions are HV-distribution, cryogenics, vacuum and heating systems. A draw-back of PCS7 is the limited support of many

[7] Depending on the charge, a particle is stored between two potential maxima or minima, within a given magnetic flux tube. In the KATRIN setup for example, a penning trap is created between the pre-spectrometer and main spectrometer.

2014 JINST 9 P06022

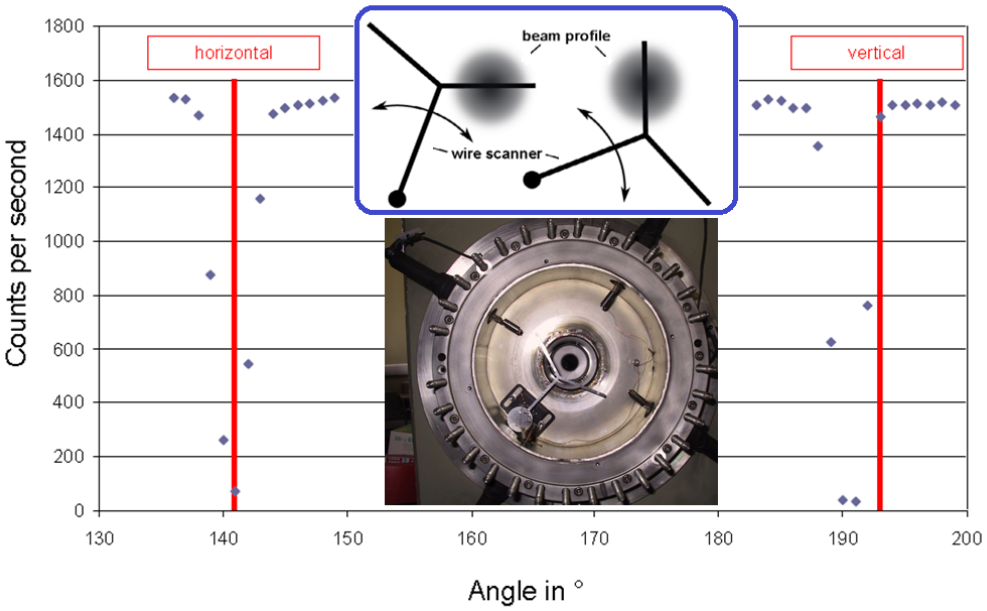

Figure 12. The picture was taken at the spectrometer center pointing towards the source section, showing the scanner and piezo motor in front of the magnet. The graphics above (blue box) depicts the operation principle for an aligned source. The sketch on the right (left) side illustrates the measurement of the horizontal (vertical) scan. When rotated, the area covered by the scanner changes as well as the beam intensity. The diagram shows the count rate in dependency of the scanner angle. In this case, the source is not fully vertically aligned. An optimal alignment of a source at $x = y = 0$ mm is indicated by the red bars.

common interfaces. To communicate to a variety of devices with different interfaces and protocols, so-called field controllers (cFP and cRio by National Instruments Inc.) are used additionally. In particular, these are high-voltage control and reading, magnetic-field monitoring, dedicated positioning devices and more. All slow-control data are collected and archived in a central database, to be available for analysis at any time. A convenient access to slow-control data is possible through the ADEI-web interface (Advanced Data Extraction Infrastructure) (ref. [30]).

Data acquisition (DAQ) is performed with ORCA (Object oriented Real time Control and Acquisition) running on Macintosh (TM of Apple Inc.) computers (ref. [31]). In the setup all hardware communication is done via Ethernet-TCP/IP. The DAQ front-end is a so-called IPE-Mini-crate-V4 equipped with a First Level Trigger (FLT) and a Second Level Trigger (SLT) card (ref. [32, 33]). The FLT digitizes the preamplifier signals without further shaping and delivers either digital traces of the signals, digital amplitudes or histograms of amplitude distributions. These data are shipped by the SLT to ORCA on the host computer for storage and on-line visualization. A process on a central server collects run data from the local machine, converts them into ROOT format (ref. [34]) and archives them. Dedicated access software is available as foundation for the development of analysis software.

Based on scripts, ORCA is used as run control to completely automate a measurement. Run lists (text files) are included in scripts, containing all required parameters (e.g. filter voltage, counting time, etc). Those set values are transfered with an ADEI-control object to the field controllers

2014 JINST 9 P06022

of the experiment.

2.7 Data analysis

For the retrieval of slow-control data and run files a program package called KaLi is available. In the raw-data analysis, the count rate in the electron peak of the detector energy-spectrum is determined and corrected for dead-time losses. For this a pulser is recorded in the same spectrum simultaneously. Also the corresponding filter voltage is retrieved, measured by 8.5-digit 8508A Fluke voltmeter connected to the K35 HV-divider. The digital voltmeter indications are corrected to the time dependent zero offset and scale factor. This results in a so-called filter plot, which is a table of count rates versus filter voltages (figure 13).

3 Results

The natural shape of the lines of a conversion-electron spectrum is Lorentzian, in case of the K-32 electrons the width γ is 2.7 eV (FWHM) (ref. [35]). A pure Lorentzian form has been observed with condensed Kr on a substrate (ref. [3, 22]), but in a solid, the structure is more complex. The sources used in this work were produced at ISOLDE (CERN), where ^{83}Rb was ion implanted into platinum substrate with 10 keV and 15 keV, respectively. Due to the implantation process, random lattice defects lead to a variation of the binding energy which can be accounted for by an additional Gaussian smearing. Outbound electrons can scatter on other electrons or atoms of the solid, they are ignored in the analysis if the energy loss is larger than 10 eV. More difficult to treat are those scattering in the conduction band only, since they cannot be separated from the no-loss electrons due to the non-negligible natural line width. Here the approach of Doniach and Šunjić (ref. [36]) is followed. The signal then is a convolution of the transmission function T of the spectrometer, the intrinsic line shape DS (a Lorentzian modified according to ref. [36]) and a Gaussian distribution G. Taking all this into account a filter plot can be described symbolically by

$$S(U,r,E,A,B,\gamma,\alpha,\sigma) = A \cdot T(U,r) \otimes DS(U,E,\gamma,\alpha) \otimes G(U,E,\sigma) + B(U), \tag{3.1}$$

where S is the signal as a function of filter voltage U, conversion-electron energy E, resolving power $r = E/\Delta E$, amplitude A, background B, natural line width γ, asymmetry parameter α and Gaussian width σ.

The signal function S is fitted with the MINUIT library (implemented in ROOT (ref. [34])) to the data in the filter plot. Details on the theoretical description and results of the filter plot involving the two fold convolution are published in a separate paper (ref. [19]).

Albeit the earth magnetic field compensation was measured, an empirical optimization showed that a different setting gives a more favorable signal-to-background ratio while the fitted line position was unchanged (figure 13). The optimized setting was used for most of the measurements. By this empirical approach for the setup of the correction coils, the imperfections in the far field of the superconducting magnet (section 2.2) can be potentially compensated.

3.1 Energy stability of the K-32 conversion line

In figure 14 the line position of the K-32-line, fitted with eq. (3.1) is shown for a data set of almost one year. Additionally to the measurements dedicated to the long-term energy stability, many

2014 JINST 9 P06022

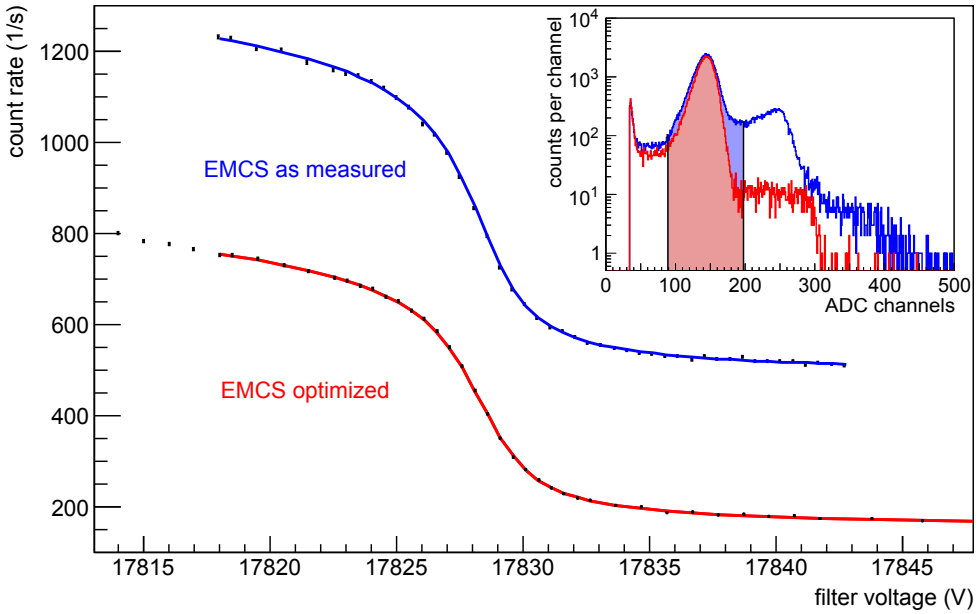

Figure 13. Filter plots obtained with the EMCS setting as determined by magnetic-field measurements (blue) and an empirical setting (red) optimized for a higher signal-to-background ratio (3.2 compared to 2.1). The colored lines are the fit result with the model given by eq. (3.1), within uncertainties the resulting line positions are the same. The insert shows electron spectra observed with the central PIN-diode when the filter voltage was set to 17816 V, that is in transmission for the no-loss electrons. The shaded areas represent the region of interest for signal electrons where all events are summed up to calculate the count rates (corrected for dead-time by means of an pulser signal) shown in the filter plot. Since no background subtraction is performed in the analysis of an ADC spectrum, a background appears in a filter spectrum and is accounted for in the fit routine.

other measurements were performed during this year[8] resulting in clustered data points. The line position values of both sources[9] were fitted over the full measurement period with a linear function, where the slope is associated with a drift of the line position of 20.3 ± 0.4 meV/month (20.8 ± 0.9 meV/month) for Pt-10-1 (Pt-15-5). Both drifts are the same within uncertainties. A linear function is used only to illustrate the long-term behavior. For the other measurements the monitor spectrometer setup was changed. Such changes are unfavorable for a long-term measurement, therefore detailed conclusions about the sources can not be drawn at this stage.

Some tests have been performed to verify that the setup is reasonably stable. To simulate a power failure, all valves were closed and the pumps were stopped for a couple of hours in the course of the routine electrical safety tests. On a warm day air conditioning was stopped, so that the lab temperature was well above 30 °C. No effect on the line position was observed.

Furthermore, the spectrometer was fully vented with ambient air at a temperature of 20 °C and a humidity of 50 %. The spectrometer was left at atmospheric pressure for 10 h, before it

[8]The measurements were mainly devoted to investigations of background reduction methods for the KATRIN main spectrometer.

[9]A source name is composed of the substrate name, the implantation energy and a consecutive number to distinguish sources produced with same properties.

2014 JINST 9 P06022

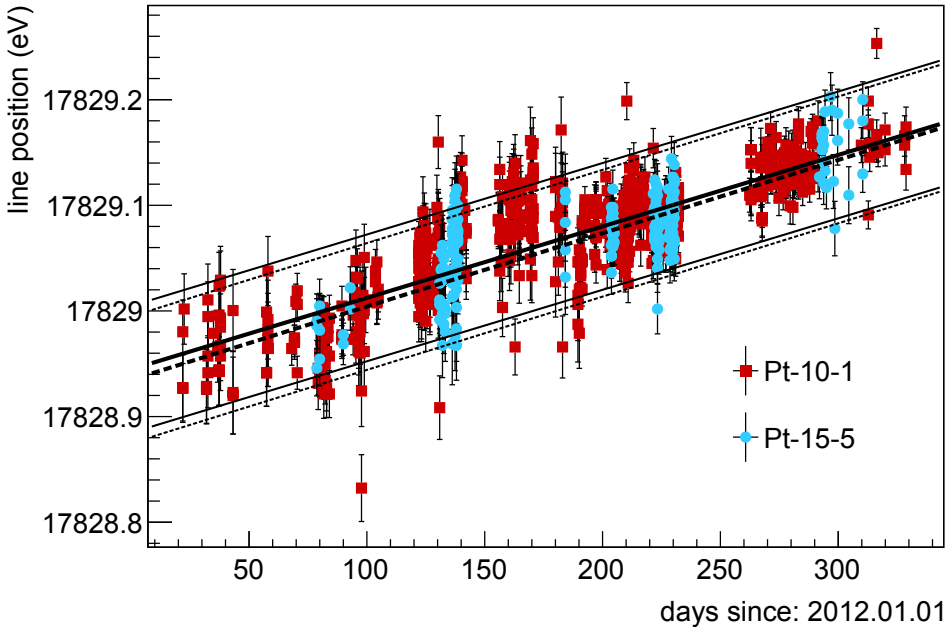

Figure 14. Time series of K-32 line positions for two different sources. For both the data were fitted with a linear function and an uncertainties band corresponding to the HV ±60 meV KATRIN requirement is plotted. For Pt-10-1 solid lines, for Pt-15-5 dotted lines are used. Voltage instability is suspected for the points which significantly deviate from the uncertainties bands. Such results would lead to an exclusion of main spectrometer data during a tritium run.

was pumped down again. In order to keep the sources under stable conditions during the venting process, the valve to the tank was closed and a pressure of $\approx 10^{-10}$ mbar was maintained in the source chamber. This venting test had a noticeable effect on the line position.

To evaluate the venting test, K-32 conversion electrons and L_{III} conversion electrons of the 9.4 keV and the 32 keV transitions were analyzed. For the three conversion lines, a reference spectrum is calculated from the average fit values of a data set from day 120 to 145, fitted with eq. (3.1). The relevant measurements were fitted with the cross-correlation method (ref. [12]), resulting in a line position relative to a reference spectrum. Figure 15 shows the deviation of the measured spectra from the corresponding reference spectra.

Data taken around day 145 and later show a shift of all three conversion line energies to lower values by 400 meV. Since the HV equipment is calibrated on a regular basis and the line position can be assumed to be stable in this short period, this effect is attributed to an increased work function of the filter electrodes caused by adsorbed residuals, especially water. According to eq. (2.3) an increased work function allows electrons with given $E_{\parallel}$ to pass the analyzing plane at a lower filter voltage $|U_f|$. The contamination with water and its removal by heating was confirmed by residual gas analysis. After heating the spectrometer to 200 °C the line positions almost recovered to their former values, but revealed an additional shift of about 80 meV to even higher values. This indicates, that the adsorbents could be removed, but maybe the filter electrode was not completely clean in the first place.

2014 JINST 9 P06022

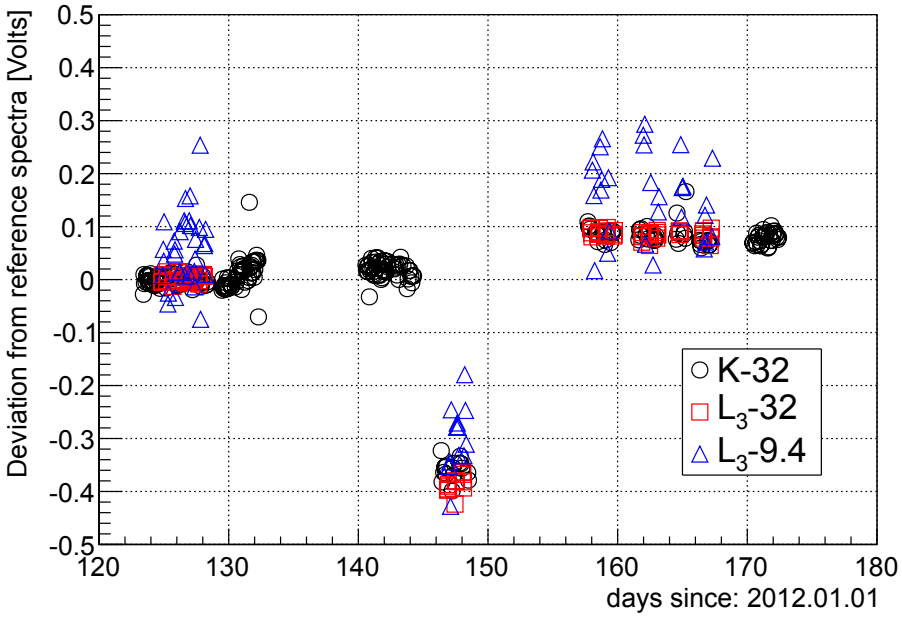

Figure 15. Detailed analyses of 3 conversion electron line positions from day 120 to 175. Beside the K-32 line, also the relative positions of the L_{III} conversion electrons of the 9.4 keV and the 32 keV transitions are included. The K-32 and L_{III}-32 lines match each other so well, that they are hard to distinguish in the diagram, whereas the position of L_{III}-9.4 line is less precise due to a poor signal to background ratio. No error bars are drawn in course not to overload the diagram.

3.2 Consequences for a KATRIN tritium run

In figure 14 1.6 % of all measured line positions deviate more than 60 meV from the KATRIN requirement for a voltage measurement, especially day 135 and 155 to 170. Assuming a Gaussian statistical fluctuation and a linear trend, line position measurements with an average uncertainty of 25 meV are expected to exceed the $\pm$60 meV range from the long-term drift in 1.2 % of all cases. In case of large deviations, tritium data will be assessed combined with voltage measurements using the K35 and K65 high-voltage dividers.

Also the measurements show a long-term trend, an increase of 200 meV in K-32 line position over a year. Moreover the trend structure can be interpreted as a combination of an overall drift and shifts at certain times. Such a behavior can have different origins.

Such a high-precision, long-term stability measurement on a ppm-level requires an accurate knowledge of the high voltage. An unstable high-voltage measurement, in particular a change of the HV-divider scale factor will cause a relative shift for all lines. This can be disentangled, since all line positions show a shift by the same absolute value (figure 15). According to calibrations in a voltage region up to 1 kV the HV-divider ratio shows a small negative drift less than -2 ppm/y (ref. [9]), confirmed by several calibrations in the high-voltage regime[10] at the Physikalisch Technische Bundesanstalt (PTB).

Changes at the level of 100 meV as observed here can be caused by a variety of solid-state physics effects in the source. A discussion of those effects is far beyond the scope of this article,

[10]Calibrations on site can be performed up to 1 kV. Calibrations at higher voltages, e.g. 18.6 kV, can only be made at the PTB.

2014 JINST 9 P06022

but will be addressed in the future. To study those effects further sources are needed with different implantation energies and doses in different substrates[11]. In cooperation with the University of Bonn those sources will be developed and tested at the monitor spectrometer.

Finally, changes of the work function of the filter electrode alter the effective analyzing voltage of the spectrometer as shown in section 3.1. This observation has consequences not only for the monitor spectrometer, but for the KATRIN main spectrometer as well. The tritium spectrum measured with the main spectrometer, is also affected by the work function of filter electrode system. The work function can behave differently from the work function of the monitor-spectrometer filter electrode and a very slow, unrecognized change of the work function over time would spoil measurements. Nevertheless, a change in the work function at the monitor spectrometer should not affect the electron measurement at the main spectrometer and vice versa. This behavior will be tested during the first commissioning of the parallel operation of both spectrometers.

But this remaining ambiguity of several 100 meV does not compromise the ability to detect a non-zero neutrino mass. By repetitive calibrations, as described in section 2.1, with a krypton source used at the main spectrometer and the monitor spectrometer, changes of the work function can be identified, but it might be necessary to perform calibrations more often than initially intended.

However, it is demonstrated that the monitor spectrometer can be used to monitor the energy scale of KATRIN for a period even longer than 2 months, the planned duration of a single KATRIN tritium run.

Acknowledgments

This work has been supported by the Helmholtz Association (HGF), the Bundesministerium für Bildung und Forschung (BMBF) with project number 05A11VK3 and 05A11PM2, the Grant Agency of the Czech Republic (GAČR) P203/12/1896 and the Deutsche Forschungsgemeinschaft (DFG) via SFB/TR 27 "Neutrinos and beyond". We also would like to thank the Karlsruhe House of Young Scientists (KHYS), the Center Elementary Particle and Astroparticle Physics (KCETA) of KIT for their support (M.E., S.G., M.K., J.R., M.Sl.). For their support of M.Sl. we also want to thank the Ministerstvo Školství, Mládeže a Tělovýchovy (MŠMT). We are grateful to the ISOLDE collaboration for giving us the opportunity to carry out the implantations of ^{83}Rb (projects I80 and IS500) and to E. Siesling for his practical help during the collections. We truly regret that our dear colleague and friend Dr. Jochen Bonn deceased shortly after the monitor spectrometer was commissioned. Without his contributions to the re-installation of the former Mainz neutrino setup in Karlsruhe, KATRIN would hardly have the well running monitor spectrometer.

References

[1] KATRIN collaboration, J. Angrik et al., *KATRIN design report 2004*, Forschungszentrum Karlsruhe GmbH, Kalrsruhe (2005), http://bibliothek.fzk.de/zb/berichte/FZKA7090.pdf, http://www.katrin.kit.edu/.

[11] It is planned to produce source with implantation energies down to 5 keV, and zinc oxide and graphite as substrates.

2014 JINST 9 P06022

[2] Particle Data Group collaboration, J. Beringer et al., *Review of particle physics*, *Phys. Rev.* **D 86** (2012) 010001.

[3] A. Picard et al., *A solenoid retarding spectrometer with high resolution and transmission for keV electrons*, *Nucl. Instrum. Meth.* **B 63** (1992) 345.

[4] Sz. Nagy, T. Fritioff, M. Björkhage, I. Bergström and R. Schuch, *On the Q-value of the tritium β-decay*, *Europhys. Lett.* **74** (2006) 404.

[5] J. Kašpar, M. Ryšavý, A. Špalek and O. Dragoun, *Effect of energy scale imperfections on results of neutrino mass measurements from β-decay*, *Nucl. Instrum. Meth.* **A 527** (2004) 423.

[6] K. Blaum, Yu. N. Novikov and G. Werth, *Penning traps as a versatile tool for precise experiments in fundamental physics*, *Contemp. Phys.* **51** (2010) 149.

[7] S. Streubel et al., *Toward a more accurate Q value measurement of tritium: status of THe-Trap*, *Appl. Phys.* **B 114** (2014) 137.

[8] M. Kraus, *Kalibration und Entwicklung von Komponenten für das KATRIN Präzisions-Hochspannungs-System*, Karlsruher Institut für Technologie (2012) diploma thesis, http://www.katrin.kit.edu/publikationen/dth-kraus-M.pdf.

[9] S. Bauer, *Kalibration und Entwicklung von Komponenten für das KATRIN Präzisions-Hochspannungs-System*, Westfälische Wilhelms-Universität Münster (2013) PhD thesis, http://repositorium.uni-muenster.de/document/miami/da3d6759-9202-4b68-bb80-711f52b208d8/diss_bauer_stephan.pdf.

[10] Th Thümmler, R Marx and Ch Weinheimer, *Precision high voltage divider for the KATRIN experiment*, *New J. Phys.* **11** (2009) 103007 [arXiv:0908.1523].

[11] S. Bauer et al., *Next generation KATRIN high precision voltage divider for voltages up to 65kV*, 2013 *JINST* **8** P10026 [arXiv:1309.4955].

[12] M. Zbořil et al., *Ultra-stable implanted ^{83}Rb/^{83m}Kr electron sources for the energy scale monitoring in the KATRIN experiment*, 2013 *JINST* **8** P03009 [arXiv:1212.5016].

[13] M. Slezák, *The source of monoenergetic electrons for the monitoring of spectrometer in the KATRIN neutrino experiment*, Charles University in Prague, NPI Řež, (2011) diploma thesis, https://www.katrin.kit.edu/publikationen/dth-slezak.pdf.

[14] A. Kovalík, V.M. Gorozhankin, A.F. Novgorodov, A. Minkova, M.A. Mahmoud and M. Ryšavý, *The K and LMX Auguer spectra of krypton from the ^{83}Rb decay*, *J. Electr. Spec. Rel. Phen.* **58** (1992) 49.

[15] S.-C. Wu, *Nuclear Data Sheets for A = 83*, *Nucl. Data Sheets* **92** (2001) 893.

[16] Ch. Kraus et al., *Final results from phase II of the Mainz neutrino mass search in tritium β decay*, *Eur. Phys. J.* **C 40** (2005) 447, [hep-ex/0412056].

[17] N. Wandkowsky, *Study of background and transmission properties of the KATRIN spectrometers*, Karlsruher Institut für Technologie (2013) PhD thesis, http://digbib.ubka.uni-karlsruhe.de/volltexte/1000036631.

[18] T. Thümmler, *Präzisionsüberwachung und Kalibration der Hochspannung für das KATRIN-Experiment*, Westfälische Wilhelms-Universität Münster (2007) PhD thesis, http://miami.uni-muenster.de/servlets/DerivateServlet/Derivate-4212/diss_thuemmler.pdf.

[19] M. Slezák et al., *Electron line shape of the KATRIN monitor spectrometer*, 2013 *JINST* **8** T12002.

[20] B. Flatt, *Voruntersuchungen zu den Spektrometern des KATRIN-Experiments*, University of Mainz (2004) PhD thesis, http://d-nb.info/975920499/34.

2014 JINST 9 P06022

[21] D. Furse et al., *Kassiopeia: A modern, extensible C++ particle tracking package*, in preparation.

[22] B. Ostrick, *Eine kondensierte ^{83m}Kr-Kalibrationsquelle für das KATRIN-Experiment*, Westfälische Wilhelms-Universität Münster (2008) PhD thesis, http://miami.uni-muenster.de/servlets/DerivateServlet/Derivate-5046/diss_ostrick.pdf.

[23] M. Zbořil, *Solid electron sources for the energy scale monitoring in the KATRIN experiment*, Westfälische Wilhelms-Universität Münster (2011) PhD thesis, http://miami.uni-muenster.de/servlets/DerivateServlet/Derivate-6323/diss_zboril.pdf.

[24] J.W. Clark, *A new method for obtaining a uniform magnetic field*, *Rev. Sci. Instrum.* **9** (1938) 320.

[25] J.E. Everett and J.E. Osemeikhian, *Spherical coils for uniform magnetic fields*, *J. Sci. Instrum.* **43** (1966) 470.

[26] S. Mertens et al., *Background due to stored electrons following nuclear decays at the KATRIN experiment and its impact on the neutrino mass sensitivity*, *Astrop. Phys.* **41** (2013) 52.

[27] Ch. Weinheimer, M. Schrader, J. Bonn, T. Loeken and H. Backe, *Measurement of energy resolution and dead layer thickness of LN2-cooled PIN photodiodes*, *Nucl. Instrum. Meth.* **A 311** (1992) 273.

[28] M. Beck et al., *Effect of a sweeping conductive wire on electrons stored in a Penning-like trap between the KATRIN spectrometers*, *Eur. Phys. J.* **A 44** (2010) 499.

[29] B. Hillen, *Untersuchung von Methoden zur Unterdrückung des Spektrometeruntergrunds beim KATRIN Experiment*, Westfälische Wilhelms-Universität Münster (2011) PhD thesis, http://miami.uni-muenster.de/servlets/DerivateServlet/Derivate-6261/diss_hillen.pdf

[30] A. Kopmann et al., *ADEI (Advanced Data Extraction Infrastracture)*, Institute for Data Processing and Electronics at Karlsruhe Institute of Technology, http://dside.dyndns.org/adei/.

[31] M.A. Howe et al., *Sudbury neutrino observatory neutral current detector acquisition software overview*, *IEEE Trans. Nucl. Sci.* **51** (2004) 878.

[32] D.G. Phillips et al., *Characterization of an FPGA-Based DAQ System in the KATRIN Experiment*, *IEEE Nucl. Sci. Symp. Conf. Rec.* (2010) 1399.

[33] A. Kopmann et al., *FPGA-based DAQ system for multi-channel detectors*, *IEEE Nucl. Sci. Symp. Conf. Rec.* (2008) 3186.

[34] R. Brun and F. Rademakers, *ROOT - An Object Oriented Data Analysis Framework*, *Nucl. Instrum. Meth.* **A 389** (1997) 81.

[35] J.L. Campbell and T. Papp, *Widths of the atomic K-N7 levels*, *At. Data Nucl. Data Tab.* **77** (2001) 1.

[36] S. Doniach and M. Šunjić, *Many-electron singularity in X-ray photoemission and X-ray line spectra from metals*, *J. Phys. C* **3** (1970) 285.

2014 JINST 9 P06022